A comprehensive analysis of quasifission lifetimes in the superheavy element region $104 \leq Z \leq 120$

G.S. Vasudha[1] D. Prakash Babu[1] N. Sowmya[2†] H.C. Manjunatha[3‡] P.S. Damodara Gupta[4]

[1]Department of Physics, REVA University, Yelahanka, Bengaluru- 560064, Karnataka, India
[2]Department of Physics, Government First Grade College, Chikkaballapura- 562101, Karnataka, India
[3]Department of Physics, Government First Grade College, Devanahalli- 562110, Karnataka, India
[4]Department of Physics, Rajah Serfoji Government College, Thanjavur- 613005, Affiliated to Bharathidasan University, Tiruchirappalli-TamilNadu

Abstract: We analyzed quasifission lifetimes of superheavy elements (SHEs) within $104 \leq Z \leq 120$ and mass number range $243 \leq A \leq 301$ considering various projectile-target combinations. Nucleus-nucleus potentials were evaluated using the nuclear proximity 2010 model, and quasifission barriers were evaluated as the difference between minimum and maximum potentials. The quasifission lifetimes varied from 0.1 zs to 2040 zs, with lifetimes above 1600 zs for $^{249}_{145}$Rf, $^{248}_{143}$Db, $^{260}_{154}$Sg, and $^{263}_{156}$Hs. The quasifission lifetimes decreased with increasing Z, dropping to 0.1 zs at Z=120. Shorter quasifission lifetimes may contribute to the reduction in production cross-sections from nanobarns to picobarns for elements with Z=104 to Z=118. Furthermore, the impact of angular momentum on quasifission barriers exhibits a decreasing trend as the atomic number increases. The shortest lifetime of 253 zs is observed at Z= 120 while longer lifetimes, such as 659 zs for ^{64}Ni+^{196}Pt, suggest enhanced stability. The model was validated against data available in literature, generally producing lower values except for ^{34}S+^{186}W, and ^{238}U+^{48}Ca, where significant increases were observed.

Keywords: quasifission barriers, quasifission lifetimes, superheavy nuclei, angular momentum

DOI: 10.1088/1674-1137/adcf10 **CSTR:**

I. INTRODUCTION

The synthesis of superheavy elements (SHE) [1] has gained considerable attention following the recent expansion of the periodic table, driven by the discovery of elements with higher atomic numbers. Under particular laboratory conditions these radioactive elements with atomic numbers greater than 103 ($Z > 103$) can only be synthesized by the fusion of two nuclei. In the formation of SHE, it is impeded by a dynamical non-equilibrium phenomenon known as quasifission [2]. In reactions involving heavy elements, quasifission (QF) and fusion-fission (FF) are the predominant processes, significantly hindering the production of an evaporation residue at higher excitation energies. Quasifission has become highly significant in heavy-ion nuclear physics due to its strong impact on compound nucleus formation and SHE synthesis [3].

Many theoretical and experimental works are going on the quasifission process. From one such theoretical results, the systematic time-dependent Hartree-Fock (TDHF) simulations of collisions was studied by Simenel et al., [4] that indicate the mass equilibration between fragments in quasi-fission had stopped. Heavy-ion reaction investigations by Godbey et al., [5] has found that the TDHF theory and its extensions were a useful theoretical tool to study quasifission. Comparing the reaction using ^{244}Pu target to the ^{239}Pu case by Guo, Lu et al., [6] showed that the quasifission was significantly decreased and the survival probability was increased by approximately one order of magnitude. Nasirov et al., [7] showed that the reduced quasifission yield were due to overlapping mass-angle distributions. Hammerton et al., [8] depicted that the dynamics of quasifission exhibit an extensive reliance on the compound nuclei N/Z. McGlynn et al., [9] reveled that the quasifission trajectories can be interpreted in terms of the underlying potential energy surface for low excitation energies.

Experimental studies on quasifission by Hinde et al., [10] revealed that the static deformation and spherical magic numbers of the colliding nuclei significantly influenced the quasifission times in collisions at energies near the capture barrier. Further Itkis et al., [11] showed that the time scale of quasifission was an indirect observable

Received 8 January 2025; Accepted 21 April 2025
† E-mail: sowmyaprakash8@gmail.com
‡ E-mail: manjunathhc@rediffmail.com

that provides insights into the intermediate stages of the SHE formation process. Quasifission typically occurs on a shorter time scale compared to compound nucleus formation. Heavy-ion reactions forming superheavy nuclei are dominated by quasifission and deep inelastic collisions, limiting compound nucleus formation. These nuclei predominantly undergo fission, revealing important formation cross-sections, fission barriers, and survival probabilities. Recent studies, focusing on mass-energy distributions via the CORSET spectrometer, provide key insights into these processes [12].

Gupta *et al.* [13] systematically studied quasifission and fusion–fission lifetimes in heavy-ion fusion reactions for superheavy elements (SHEs) synthesis show longer quasifission lifetimes in successful reactions. The performance lifetimes depend on the energy, the angular momentum, and deformation parameters. Manjunatha *et al.* [14] studied quasifission and fusion-fission lifetimes for Z=120 synthesis were analyzed using the dinuclear system model. Further the influence of projectile-target orientation and angular momentum on quasifission barriers has been investigated Gupta *et al.* [15] in detail and also investigated Coulomb fission and quasifission lifetimes [16].

The synthesis of SHEs continues to challenge nuclear physicists, with quasifission (QF) being a significant barrier in the formation of compound nuclei. Despite extensive theoretical and experimental studies, many aspects of the quasifission process remain poorly understood, motivating further investigation. Identifying optimal projectile-target combinations, beam energies, and orientation angles is essential for minimizing quasifission and maximizing fusion probabilities, which is crucial for achieving measurable evaporation residue cross-sections. To facilitate the synthesis of superheavy elements (SHEs), it is important to gain a comprehensive understanding of quasifission mechanisms. A systematic study of quasifission lifetimes across the SHE region ($104 \leq Z \leq 120$) is necessary to enhance the prediction of reaction dynamics and optimize experimental conditions. A detailed investigation into these aspects will provide critical insights into the dynamics of SHE formation and improve strategies for successful synthesis.

II. THEORETICAL FRAMEWORK

The dinuclear system's nucleus-nucleus interaction potential [17] is expressed as

$$V(R,Z_i,\beta_{2i},\ell) = V_c(R,Z_i,\beta_{2i}) + V_N(R,Z_i,\beta_{2i}) + V_{rot}(\ell,\beta_{2i}). \quad (1)$$

Here, $i = 1,2$, identifies whether the parameter belongs to the projectile (i = 1) or target (i = 2) in which Z_i accounts for atomic number of nucleus i, and β_{2i} corresponds to Quadrupole deformation parameter of nucleus i which accounts for nuclear shape effects. R represents the distance between the two centers, $V(R,Z_i,\beta_{2i},\ell)$ denotes the nucleus-nucleus potential, V_C corresponds to the Coulomb potential, V_N is the nuclear potential, and V_{rot} signifies the rotational potential. The terms V_C, and V_{rot} are evaluated using set of equations explained in [14,17]. The term V_N is evaluated as explained in literature [18] in which proximity 2010 potential has been taken in the evaluation of the nuclear potential.

The quasifission lifetime of an excited asymmetric dinuclear system (DNS) [14,17,19] is given by;

$$\tau_{qf} = \frac{1}{\lambda_{qf}}, \quad (2)$$

here λ_{qf} represents the quasifission decay constant, expressed as:

$$\lambda_{qf} = \frac{\omega_m}{2\pi\omega_{qf}}\left(\sqrt{\left(\frac{\Gamma}{2\hbar}\right)^2+\omega_{qf}^2}-\frac{\Gamma}{2\hbar}\right) \exp\left(-\frac{B_{qf}(Z,A,\ell)}{\Theta_{DNS}(Z,A)}\right) \quad (3)$$

The term Γ denotes the average width of the single-particle states near the Fermi surface, typically taken as 2 MeV. ω_m, and ω_{qf} represent the frequencies of the harmonic oscillator and the inverted harmonic oscillator, respectively [14]. The quasifission barrier ($B_{qf}(Z,A,\ell)$) in the dinuclear system is given by:

$$B_{qf}(Z,A,l) = V(R_b,Z,A,\beta_{2i},\ell) - V(R_m,Z,A,\beta_{2i},\ell) \quad (4)$$

where ℓ is the angular momentum. The term β_{2i} is the quadrupole deformation parameter of projectile and target, whose values have been taken reference [20,21]. R_m and R_b are the distance at which the potential is minimum and maximum in the DNS system. The nucleus-nucleus potential is minimum at distance $R = R_m$ [17]. The local temperature Θ_{DNS} is expressed as;

$$\Theta_{DNS}(Z,A) = \sqrt{\left(\frac{E_{DNS}-B_{qf}}{a}\right)}. \quad (5)$$

The excitation energy of DNS is expressed as

$$E_{DNS} = E_{cm} - V(R_m) \quad (6)$$

where E_{cm} is the center of mass energy.

III. RESULTS AND DISCUSSIONS

We investigated quasifission lifetimes of SHEs in the region $104 \leq Z \leq 120$ and mass number region $243 \leq A \leq 301$. In this view we considered different projectile-target combinations. For the projectile, the selected atomic and mass number is between $20 \leq Z \leq 30$ and $40 \leq A \leq 70$ respectively. Similarly, the target's atomic and mass number ranges between $74 \leq Z \leq 98$, and $180 \leq A \leq 252$ respectively. Likewise, we studied about 1946 fusion reactions in the SHEs in the region $104 \leq Z \leq 120$. For each projectile-target combination, the nucleus-nucleus potential is evaluated by keeping orientation angle $\alpha_1 = 90^0$ and $\alpha_2 = 90^0$. Figure 1 show a plot of the nucleus-nucleus interaction potential of the dinuclear system with the mean distance between their centers. The studied nucleus-nucleus potential is specifically for the reaction ^{45}Sc+^{209}Bi, and different curves have been plotted for different values of angular momentum ($\ell = 0, 2, 4, 6, 8, 10, 12$). The total potential decreases as R increases, showing the behavior of the nucleus-nucleus interaction potential where the repulsive Coulomb and attractive nuclear forces interact. As ℓ increases, the potential barrier shifts upward, indicating a centrifugal effect due to angular momentum. In addition the barrier height increases with ℓ which is consistent with the additional rotational energy introduced by higher angular momentum.

Once, the minimum and maximum potentials were identified, then the quasifission barriers were evaluated using equation (4). For instance, we have plotted effect of angular momentum on quasifission barriers for the fusion reaction of ^{45}Sc+^{209}Bi and it is presented in figure 2. As ℓ increases the B_{qf} gradually decreases. The values of B_{qf} range approximately between 4.84 MeV and 4.72 MeV, showing a relatively small variation over the entire range of ℓ.

For each isotope, we get different projectile-target combinations. For the formation of compound nuclei ^{246}Rf, we considered possible 8 projectile-target combinations such as ^{52}Cr+^{194}Hg, ^{50}Cr+^{196}Hg, ^{56}Fe+^{190}Pt, ^{62}Ni+^{184}Os, ^{60}Ni+^{186}Os, ^{58}Ni+^{188}Os, ^{66}Zn+^{180}W, and ^{64}Zn+^{182}W. The quasifission barriers obtained for these studied fusion reactions were plotted as shown in figure 3. The B_{qf} were observed to be larger for ^{66}Zn+^{180}W when compared to other studied fusion reactions. Similarly, smaller B_{qf} is noticed for ^{56}Fe+^{190}Pt fusion reaction. The larger B_{qf} values are more favorable for synthesizing superheavy elements, as they resist quasifission and enhance fusion probability. On the other hand, the smaller values B_{qf} correspond to the reactions where the likelihood of quasifission is the highest. Hence, in each isotope we have identified larger B_{qf} values.

We identified larger B_{qf} values for fusion reactions forming Rutherfordium (Rf) isotopes (Z=104). Approximately 190 fusion reactions were analyzed for the production of isotopes ranging from ^{242}Rf to ^{260}Rf. Figure 4 depicts the variation of the quasifission barrier, B_{qf}, as a function of the compound nuclei's mass numbers. The analysis reveals a general trend where B_{qf} increases with the mass number of the compound nuclei, reaching a peak value of 8.5 MeV for $^{249}_{145}$Rf. This maximum value is notably higher than those of neighboring nuclei, indicating enhanced stability against quasifission. Following this maximum, B_{qf} gradually decreases with increasing mass number. However, secondary maxima are observed at $^{246}_{142}$Rf with 7.98 MeV and $^{252}_{148}$Rf with 8.23 MeV, suggesting regions of increased stability in these nuclei. Further-

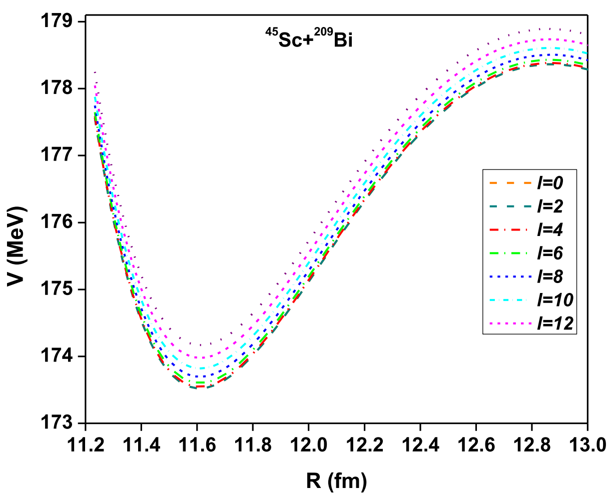

Fig. 1. (color online) The variation of nucleus-nucleus interaction potential of the dinuclear system with the mean distance between their centers for different angular momentum and orientation angles of projectile and target were fixed at $\alpha_1 = 90^0$, and $\alpha_2 = 90^0$.

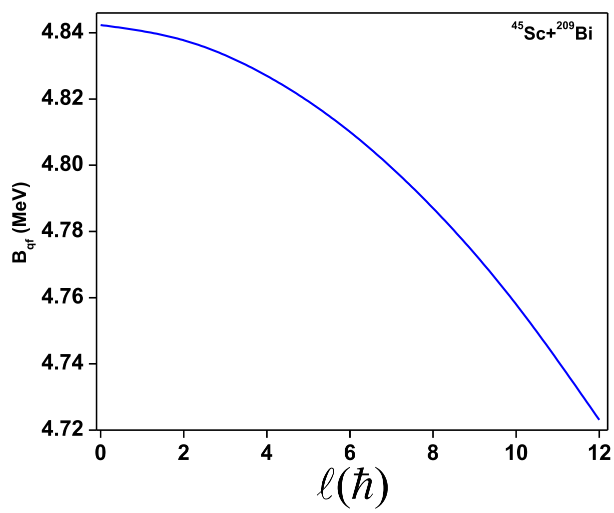

Fig. 2. (color online) A plot of quasifission barrier as a function of angular momentum for the fusion reaction of ^{45}Sc+^{209}Bi.

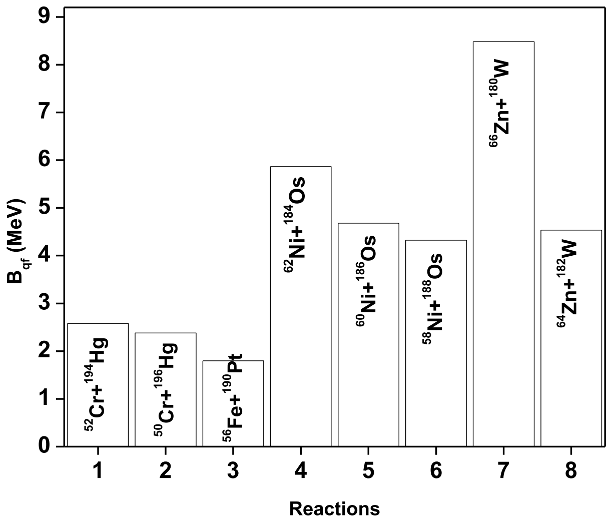

Fig. 3. A comparison of quasifission barriers for the fusion reactions leading to form ^{246}Rf.

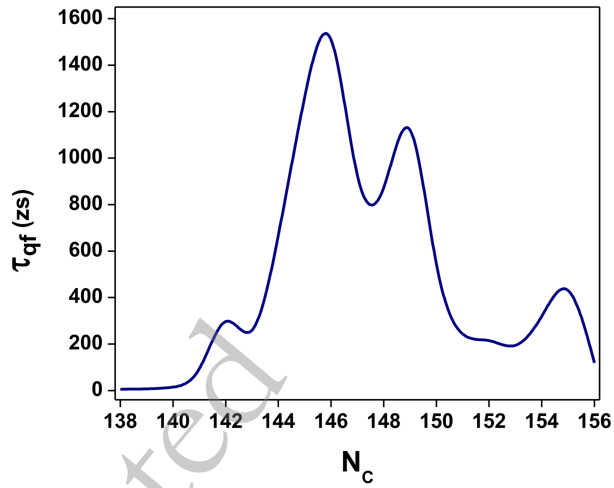

Fig. 5. (color online) A plot of quasifission lifetimes obtained for the fusion reactions forming Rutherfordium (Rf) isotopes (Z=104).

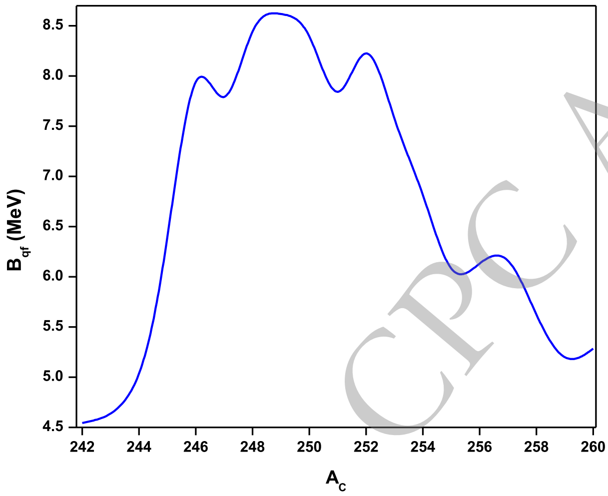

Fig. 4. (color online) A plot of larger quasifission barriers obtained for the fusion reactions leading to form an isotopes of ^{242}Rf to ^{260}Rf as a function of mass number of compound nuclei.

more, a third maximum is identified at $^{257}_{153}$Rf with a B_{qf} value of 6.22 MeV. These distinct maxima reflect variations in the quasifission barrier with respect to a mass number of compound nuclei.

Furthermore, the quasifission lifetimes were evaluated using equation (3). The lifetime of the quasifission process is typically in the range of 10^{-20} to 10^{-18} seconds. Figure 5 shows a plot of quasifission lifetimes obtained for the fusion reactions forming Rutherfordium (Rf) isotopes (Z=104) as a function of neutron number of compound nuclei. The evaluated quasifission lifetimes were in the range of 0.1zs to 1600zs. The larger lifetimes were observed when $N_c = 145$ which corresponds to $^{249}_{145}$Rf nuclei which has larger quasifission barrier with 8.5 MeV as seen in figure 4. Similarly, second maxima is noticed when $N_c = 142, 148$. But further a maxima is observed when $N_C = 155$, which is slightly shifted towards larger N_c. But, the larger B_{qf} is noticed when $N_c = 153$ as seen in figure 4. Which may be due to additional terms involved in the evaluation of ω_m, ω_{qf} and local temperature $\Theta_{DNS}(Z,A)$. However, this effect is less observed in case of $N_c = 142, 145, 148$. Longer quasifission lifetimes indicate that the composite system stays in contact for a relatively extended period, allowing more time for the system to dissipate energy and angular momentum. This is often associated with a higher quasifission barrier (B_{qf}) and increased stability against fission. Shorter lifetimes, on the other hand, suggest rapid re-separation, often linked to lower B_{qf}-values and less favorable conditions for fusion. The larger Peak in the quasifission barrier observed in case of $^{249}_{145}$Rf, with longer quasifission lifetimes, enhances the likelihood of compound nucleus formation.

Further, Similar investigations were carried out in the formation of compound nuclei in the superheavy region $105 \leq Z \leq 120$. In each isotope, we have identified larger B_{qf}. The map 6 showcases the quasifission barriers (B_{qf}) for different combinations of projectile and target atomic numbers that result in compound nuclei within the atomic number range $104 \leq Z \leq 120$. The lower quasifission barriers ranges from 0 MeV to 3.464 MeV which is represented by purple to dark cyan. However, higher B_{qf} were observed up to 8.66 MeV which varies between light cyan to red color. The larger quasifission barriers were observed when $N_c > 161$. In addition, we noticed larger B_{qf} when Z=104 to 106, and for Z=114 the larger B_{qf} above 6 MeV were observed. We also observed that as the neutron number of each Z increases the quasifission barriers also increases particularly for $Z > 108$. For an instance, neutron number of compound nuclei (N_c) varies from 143 to 168 with Z=108. Here the quasifis-

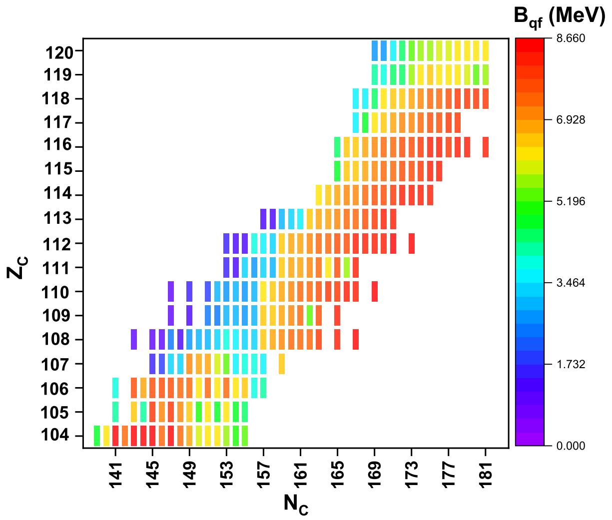

Fig. 6. (color online) A map illustrating the quasifission barriers (B_{qf}) for various combinations of projectile and target atomic numbers, leading to the formation of compound nuclei within the atomic number range $104 \leq Z \leq 120$, is presented. The map uses a color gradient, where an increase in B_{qf} values is represented by a transition from purple to red regions.

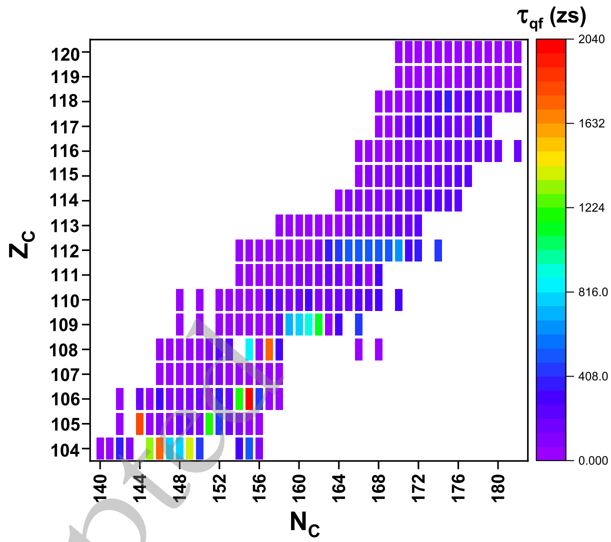

Fig. 7. (color online) A map illustrating the quasifission lifetimes for various combinations of projectile and target atomic numbers, leading to the formation of compound nuclei within the atomic number range $104 \leq Z \leq 120$, is presented. The map uses a color gradient, where an increase in τ_{qf} values is represented by a transition from purple to red regions.

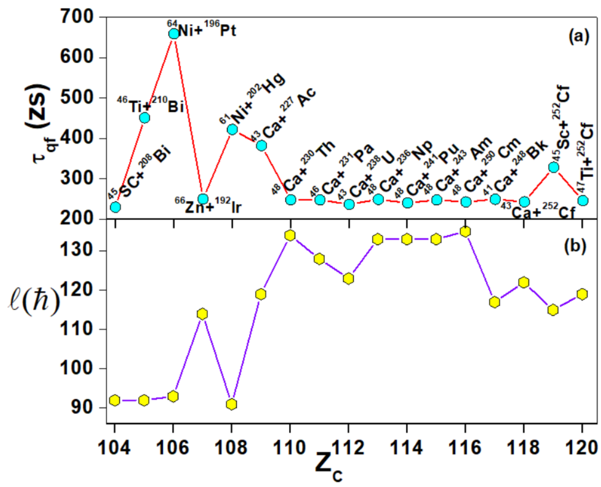

Fig. 8. (color online) (a) A plot of larger quasifission lifetimes, and (b) angular momentum as a function of compound nuclei's atomic number in the range $104 \leq Z \leq 120$.

sion barriers ranges between 1.7 MeV to 8.66 MeV which is clearly represented by blue to red color.

Furthermore, we have identified the larger quasifission lifetimes in each isotope of compound nuclei ranging between $104 \leq Z \leq 120$ and it is portrayed in heat map 7. From the map it is observed that the lifetimes varies between 0.1 zs to 2040 zs these lifetimes have been represented by purple to red color. Above 1632 zs were observed for $^{249}_{145}$Rf, $^{248}_{143}$Db, $^{260}_{154}$Sg, and $^{263}_{156}$Hs. However, in all other cases the quasifission lifetimes were less than 1632 zs.

Further, we plotted angular dependent quasifission lifetimes for each atomic number as seen in figure 8(a). The plot reveals a gradual decrease in quasifission lifetimes with increasing atomic number of the compound nuclei. For Z=120, the lifetimes diminish to as low as 253 zs, indicating reduced stability against quasifission as atomic number increases. However, a larger quasifission lifetimes were observed for ^{64}Ni+^{196}Pt leading to form the compound nuclei $^{260}_{106}$Sg with the quasifission lifetime of 659 zs. Further, a larger quasifission lifetimes were also observed for ^{46}Ti+^{210}Bi, ^{61}Ni+^{202}Hg, ^{43}Ca+^{227}Ac, and ^{45}Sc+^{252}Cf fusion reactions. The corresponding angular momentum values have been plotted in figure 8(b). Here the angular momentum is varied between 91$\hbar$ to 135$\hbar$. The lowest value of 91$\hbar$ is observed for the reaction of ^{61}Ni+^{202}Hg, similarly, higher value of 135$\hbar$ is observed for ^{48}Ca+^{250}Cm reaction. These ℓ-values have been taken from the Nuclear video project [22].

Furthermore, the model has been tested by comparing quasifission lifetimes with the experimentally available data [23,24] which is tabulated in Table 1. From the comparison it has been observed that the present work (PW) values are generally lower than those in the references, except for some reactions ^{34}S+^{186}W and ^{238}U+^{48}Ca where PW reports significantly larger lifetimes. For reactions with ^{238}U as a target, the PW values are closer to the literature but still show systematic differences. In case of ^{48}Ti+^{186}W, a reduction in PW values by half. In case of ^{34}S+^{186}W and ^{238}U+^{48}Ca a significant increase in quasifission lifetimes is observed in the PW compared to the literature. For ^{238}U+^{64}Ni, ^{238}U+^{58}Fe, and ^{238}U+^{48}Ti, the PW

Table 1. A comparison of quasifission lifetimes obtained using present work with that of experimentally available data [23,24].

Reaction	E_{cm} (MeV)	ℓ	$\tau_{qf}(zs)$	
			Ref.	PW
^{48}Ti+^{186}W	245	124	10[23]	5
^{64}Ni+^{184}W	341	124	5[23]	1.01
^{34}S+^{186}W	180	116	10[23]	55.25
^{238}U+^{27}Al	146	113	≈12.7[24]	2.5
^{238}U+^{48}Ca	216	135	3.7[24]	31.5
^{238}U+^{45}Sc	227	122	3.2[24]	8.5
^{238}U+^{48}Ti	240	123	2.9[24]	5.25
^{238}U+^{58}Fe	280	118	2.6[24]	1.25
^{238}U+^{64}Ni	303	115	2.5[24]	1.26

values are lower and closely aligned with literature values, indicating some consistency with the present model. The discrepancies between theoretical and experimental quasifission lifetimes arise due to several key limitations in the present model. The study employs the nuclear proximity 2010 model, which, while effective, does not fully capture dynamical effects, shell structure influences, and nucleon transfer mechanisms that significantly impact quasifission. Additionally, quasifission lifetimes are derived using a decay constant approach, assuming a well-defined transition from the dinuclear system to quasifission. However, real reactions involve stochastic fluctuations in mass and angular distributions, leading to deviations from measured lifetimes. Further, in our study we also considered a fixed nuclear orientation ($\alpha_1 = 90^0$ and $\alpha_2 = 90^0$) and does not fully account for orientation-dependent fusion probabilities, which are crucial for deformed nuclei. Furthermore, shell corrections and energy dissipation mechanisms are not explicitly included, though experiments suggest they strongly influence quasifission barriers. From the figure 8 we observed smaller lifetimes corresponding to ^{48}Ca-induced fusion reactions, but these corresponding lifetimes were found to be smaller when compared to neighboring nuclei. This suggests a distinct behavior in fusion dynamics for ^{48}Ca-induced reactions, and also experimentally[25] it has been observed that the evaporation residue cross-sections corresponding to these superheavy elements are in the range of picobarn (pb). Hence, this may be also one of the fact that as quasifission lifetimes decrease, the production cross-sections reduce from nb to pb in the region Z=104 to 118.

IV. CONCLUSIONS

We investigated the quasifission lifetimes of superheavy elements (SHEs) in the atomic number range $104 \le Z \le 120$ and mass number range $243 \le A \le 301$. To achieve this, we considered various projectile-target combinations. The projectiles selected had atomic numbers in the range $20 \le Z \le 30$ and mass numbers between $40 \le A \le 70$. Similarly, the targets had atomic numbers ranging from $74 \le Z \le 98$ and mass numbers between $180 \le A \le 252$. The nucelus-nucleus potential is evaluated by considering nuclear proximity 2010. The quasifission barriers have been evaluated by taking difference between minimum and maximum potential. The quasifission barrier is found to be maximum at $\ell = 0$. Furthermore, quasifission barriers and lifetimes were evaluated in the fusion reactions leading to form compound nuclei in the superheavy region $104 \le Z \le 120$. A heat map (Figure 7) of quasifission lifetimes for compound nuclei ($104 \le Z \le 120$) revealed lifetimes ranging from 0.1 zs to 2040 zs, represented by purple to red. Lifetimes above 1600 zs were identified for $^{249}_{145}$Rf, $^{248}_{143}$Db, $^{260}_{154}$Sg, and $^{263}_{156}$Hs, while others were below 1600zs. The quasifission lifetimes shows a gradual decrease in lifetimes with increasing atomic number, reducing to 0.1 zs for Z=120, indicating a decline in stability against quasifission with higher atomic numbers. Furthermore, the influence of angular momentum on quasifission barriers showing a decline with increasing atomic number. The shortest lifetime of 253 zs occurs at Z=120, while longer lifetimes, such as 659 zs for ^{64}Ni+^{196}Pt, indicate greater stability. The present model was validated by comparing quasifission lifetimes with available data. PW values are generally lower than references, except for ^{34}S+^{186}W and ^{238}U+^{48}Ca, showing significant increases. For ^{238}U-based reactions, PW aligns better, though systematic differences exist.

References

[1] M. Schädel, Radiochimica Acta **100**, 579 (2012)

[2] M. G. Itkis, A. A. Bogachev, I. M. Itkis, J. Kliman, G. N. Knyazheva, N. A. Kondratiev, E. M. Kozulin, L. Krupa, Y. Ts. OGANESSIAN, I. V. Pokrovsky, *et al.*, The processes of fusion-fission and quasi-fission of superheavy nuclei, in *Dynamical Aspects of Nuclear Fission* (World Scientific, 2008) pp. 36–53.

[3] G. Mohanto, D. J. Hinde, K. Banerjee, M. Dasgupta, D. Y. Jeung, C. Simenel, E. C. Simpson, A. Wakhle, E. Williams, I. P. Carter, *et al.*, Physical Review C **97**, 054603 (2018)

[4] C. Simenel, P. McGlynn, A. S. Umar, and K. Godbey, Physics Letters B **822**, 136648 (2021)

[5] K. Godbey and A. S. Umar, Frontiers in Physics **8**, 40 (2020)

[6] L. Guo, C. Shen, C. Yu, and Z. Wu, Physical Review C **98**, 064609 (2018)

[7] A. K. Nasirov, G. Giardina, G. Mandaglio, M. Manganaro, F. Hanappe, S. Heinz, S. Hofmann, A. I. Muminov, and W.

Scheid, Physical Review C—Nuclear Physics **79**, 024606 (2009)
[8] K. Hammerton, Z. Kohley, D. J. Hinde, M. Dasgupta, A. Wakhle, E. Williams, V. Oberacker, A. S. Umar, I. P. Carter, K. Cook, *et al*., Physical Review C **91**, 041602 (2015)
[9] P. McGlynn and C. Simenel, Physical Review C **107**, 054614 (2023)
[10] D. J. Hinde, M. Dasgupta, and E. C. Simpson, Progress in Particle and Nuclear Physics **118**, 103856 (2021)
[11] M. G. Itkis, E. Vardaci, I. M. Itkis, G. N. Knyazheva, and E. M. Kozulin, Nuclear Physics A **944**, 204 (2015)
[12] M. G. Itkis, G. N. Knyazheva, I. M. Itkis, and E. M. Kozulin, The European Physical Journal A **58**, 178 (2022)
[13] P. S. D. Gupta, H. C. Manjunatha, N. Sowmya, and T. Ganesh, Pramana **96**, 214 (2022)
[14] H. C. Manjunatha, L. Seenappa, P. S. Damodara Gupta, N. Manjunatha, K. N. Sridhar, N. Sowmya, and T. Nandi, Physical Review C **103**, 024311 (2021)
[15] P. S. Damodara Gupta, N. Sowmya, H. C. Manjunatha, L. Seenappa, and T. Ganesh, Physical Review C **106**, 064603 (2022)
[16] T. Nandi, H. C. Manjunatha, P. S. D. Gupta, N. Sowmya, N. Manjunatha, K. Sridhara, and L. Seenappa, Pramana **96**, 230 (2022)
[17] S. Soheyli and M. V. Khanlari, Physical Review C **94**, 034615 (2016)
[18] H. C. Manjunatha and N. Sowmya, Nuclear Physics A **969**, 68 (2018)
[19] Khanlari, M. Varasteh, and S. Soheyli, Physical Review C **95**, 024617 (2017)
[20] P. Moller, J. Nix, W. Myers, and W. Swiatecki, Atomic Data and Nuclear Data Tables **59**, 185 (1995)
[21] Reference input parameter library (ripl-3), https: //www-nds.iaea.org/RIPL-3.html.
[22] Nrv video project, ttp: //nrv.jinr.ru/nrv/webnrv/fusion/reactions.tml.
[23] R. du Rietz, D. J. Hinde, M. Dasgupta, R. G. Thomas, L. R. Gasques, M. Evers, N. Lobanov, and A. Wakhle, Phys. Rev. Lett. **106**, 052701 (2011)
[24] J. Toke, R. Bock, G. X. Dai, A. Gobbi, S. Gralla, K. D. Hildenbrand, J. Kuzminski, W. F. J. Müller, A. Olmi, H. Stelzer, *et al*., Nuclear Physics A **440**, 327 (1985)
[25] S. Hofmann and G. Münzenberg, Reviews of Modern Physics **72**, 733 (2000)